Applied Nanoscience (2023) 13:5421–5433
https://doi.org/10.1007/s13204-023-02822-5

ORIGINAL ARTICLE

A comparative study of iron nanoflower and nanocube in terms of antibacterial properties

Ozan Eskikaya[1] · Sadin Özdemir[2] · Serpil Gonca[3] · Nadir Dizge[1] · Deepanraj Balakrishnan[4] · Feroz Shaik[4] · Natarajan Senthilkumar[5]

Received: 13 November 2022 / Accepted: 5 March 2023 / Published online: 5 April 2023
© King Abdulaziz City for Science and Technology 2023

Abstract
It is known that heavy metal containing nanomaterials can easily prevent the formation of microbial cultures. The emergence of new generation epidemic diseases in the last 2 years has increased the importance of both personal and environmental hygiene. For this reason, in addition to preventing the spread of diseases, studies on alternative disinfectant substances are also carried out. In this study, the antibacterial activity of nanoflower and nanocube, which are easily synthesized and nanoparticle species containing iron, were compared. The antioxidant abilities of new synthesized NF@FeO(OH) and NC@α-Fe_2O_3 were tested by DPPH scavenging activity assay. The highest DPPH inhibition was achieved with NC@α-Fe_2O_3 as 71.30% at 200 mg/L. NF@FeO(OH) and NC@α-Fe_2O_3 demonstrated excellent DNA cleavage ability. The antimicrobial capabilities of NF@FeO(OH) and NC@α-Fe_2O_3 were analyzed with micro dilution procedure. In 500 mg/L, the antimicrobial activity was 100%. In addition to these, the biofilm inhibition of NF@FeO(OH) and NC@α-Fe_2O_3 were investigated against *S. aureus* and *P. aeruginosa* and it was found that they showed significant antibiofilm inhibition. It is suggested that additional studies can be continued to be developed and used as an antibacterial according to the results of the nanoparticles after various toxicological test systems.

Keywords Nanoflower · Nanocube · DNA cleavage · Antimicrobial activity · Microbial cell viability · Biofilm inhibition

Introduction

Nanotechnology is defined as a design with shape and size with scale 1 nm and 100 nm, which is used in many areas, such as characterization, devices and systems controls (Yin et al. 2020). Nanotechnology has a good number of applications including nanoparticles and nanomaterials (Li et al. 2021) (nanoflower, nanocubes etc.) (Lei et al. 2021; Clark et al. 2019), nanomembranes (Puri et al. 2021), nanosensors (Sharma et al. 2021) and nanorobots (Zhou et al. 2021) have been produced. Porous nanoparticles not only have a bigger surface, but in addition improve physicochemical properties. It has really been demonstrated that they are useful in lots of areas, including sensing, catalysis, separation, and storage applications (Subramani et al. 2021). Nanoparticles have a wide range of use, because they are nano-sized, they provide volume advantages, they have a reactive structure and they have antibacterial properties (Martín-Moreno et al. 2020). Nanomaterials are thought to be effective adsorbents. Nanomaterials are used as catalysts because of their wide variety of applications, shorter distance for interparticle diffusion, low temperature modification, varied pore size, and surface chemistry benefits over other materials (Okejiri et al. 2020). Nanoparticle has been studied for different purposes cancer and tumor delivery (Alhallak et al. 2021; Ouyang et al. 2020), pharmaceutical industry (Cevaal et al. 2021), energy storage and transfer

✉ Nadir Dizge
ndizge@mersin.edu.tr

✉ Deepanraj Balakrishnan
babudeepan@gmail.com

1 Department of Environmental Engineering, Mersin University, 33343 Mersin, Turkey

2 Technical Science Vocational School, Mersin University, Yenisehir, 33343 Mersin, Turkey

3 Faculty of Pharmacy, University of Mersin, Turkey, Yenisehir, 33343 Mersin, Turkey

4 College of Engineering, Prince Mohammad Bin Fahd University, Al Khobar 31952, Saudi Arabia

5 Saveetha School of Engineering, Saveetha Institute of Medical and Technical Sciences, Chennai 602105, India

(Kumar et al. 2021; Pramanik et al. 2021), as a biosensor (Vizzini et al. 2021), the construction of sensors for technological purposes (Aslanidis et al. 2021), and wastewater treatment (El-Shafai et al. 2021), which can be exemplary studies.

Nanoflower (NF) is a newly developed type of nanoparticle class for various purposes. It has a just like plant flowers that possess a nanoscale framework between 100 and 500 nm. The general properties of nanoflowers accelerate the reaction kinetics and reaction efficiency due to its 3D structure, it is combined with different materials, it has simple and cost-effective synthesis methods (Zhang et al. 2021). Another nanomaterial is nanocubes, because its shape is similar to cubes. Nanocubes (NC) are an innovative material as other nanoparticles. Nanocubes with 3D structure are newly used in different application areas (Sun et al. 2021; Mimura and Kato 2020). Rahmati et al. (2021) have produced an electrochemical biosensor with the nanocube device to speed up the early detection of protein detection of SARS-CoV-2. The nanocubes used in the study, having a large surface area in a small area, were able to achieve early diagnosis with a small amount of saliva sample.

Various research groups have synthesized nanomaterial using different chemicals, such as Fe (Ekata et al. 2020), Ni (Duan et al. 2021), Zn (Ekennia et al. 2021), Cu (Hu et al. 2021), Ti (Harris et al. 2020) etc. Metallic nanoparticles are frequently used in applications such as catalysis, sensing, optics, energy storage and antimicrobial due to their chemical structure and unique size and shape (Shahabadi et al. 2021). Nanomaterials produced with iron, which is a heavy metal group, are very useful in such application areas (Cabana et al. 2020). The oxide and (oxy) hydroxide of iron (Fe_3O_4 and FeOOH) have been shown to be beneficial in various fields. Among the wide variety of iron oxides, there are types, such as α-, β- and γ-types. These iron oxyhydroxide (FeOOH) species are synthesized by different production methods. Nanomaterials such as these, materials with magnetic fields, are used quite efficiently for a variety of applications. Goethite (α-FeOOH), which occurs naturally in soil and iron ore, has interesting magnetic properties and is an abundant mineral (Huang et al. 2020; Wan et al. 2017). One of the iron-containing materials is iron (III) oxide-hydroxide ($Fe(OH)_3$), hydroxyl ions are added into the solution containing Fe^{3+} ions and $Fe(OH)_3$ is synthesized by reacting (Niu et al. 2021). Iron (III) oxide-hydroxide has been widely used in heavy metal removal for a long time. In a study by Pham et al. (2020) successfully purified arsenate, a type of arsenic, from drinking water with nanoflower type α-FeOOH. They determined that the adsorption capacity of nanoflower was 475 μg/g. Liu et al. (2021), examined the antibacterial activity of goethite type nanoflowers in their study. In their study, they determined that it caused RNA and membrane damage on *E.coli* bacteria. Supermagnetic materials such as magnetite (Fe_3O_4) and its oxidized form maghemite (γ-Fe_2O_3) are promising materials for biomedical applications due to their various properties. They've recently been widely employed in medication delivery systems to transport a variety of substances, as well as in a variety of other fields (Gabrielyan et al. 2020). Iron oxide, among the numerous metal oxides, emerges as a potential material due to its low cost, ease of production, and environmental friendliness. Fe_2O_3 nanoparticles have been synthesized by hydrothermal. Iron oxide exhibits various forms, such as maghemite (γ-Fe_2O_3), akaganeite (β-Fe_2O_3), hematite (α-Fe_2O_3), and ε-Fe_2O_3 (Xu et al. 2021). Karthika (2021) reported that iron-containing nanomaterial shows antibacterial activity towards *Escherichia coli* and *Staphylococcus aureus* bacteria. In their study, they aimed to use iron-containing nanomaterial as an implant. It has been determined that the nanomaterial obtained in the study can be beneficial for bone formation and tissue regeneration when used in advanced implant applications. Mohammad et al. (2020) constructed a flower-like structure in which they reported the superantimicrobial activity of *E. coli*. They used iron and silicon as inorganic compounds for the synthesized nanoflower. It may lead to the use of the compound obtained with this feature, which has superantimicrobial properties, in the health sector.

In this study, it was desired to compare the antibacterial properties of nanoparticles synthesized by two different methods. One of the synthesized iron-containing nanoflower materials was obtained at low temperature. It was named NF@FeO(OH) for the sample. Another synthesized nanocubes was named NC@α-Fe_2O_3. Nanocubes were synthesized under high temperature and pressure. The characterization of the nanoparticles obtained as a result of the study was obtained by various spectroscopic tools including XRD, SEM and EDX their antimicrobial activities were examined.

Materials and methods

Materials

Urea ($CO(NH_2)_2$, > %99.5), Iron (II) sulfate heptahydrate pure ($FeSO_4.7H_2O$) and Iron (III) chloride ($FeCl_3$, > %98). All chemical was purchased from Sigma-Aldrich. Two-stage Millipore Direct-Q_3 was used to produce distilled water.

Nanoflowers synthesis

NF@FeO(OH) was revised and synthesized using the hydrothermal method (Raul et al. 2014). Briefly, 6.95 g (0.1 M) $FeSO_4.7H_2O$ was prepared in a 250 mL beaker with DI. The solution was heated to 60 °C with constant stirring. Stirring was continued for 30 min when the temperature rises to 60 °C. 5 M urea solution pre-dissolved in 250 mL of distilled water was added dropwise to this solution for 3.5 h. During the addition of the urea solution in the iron-containing solution, the temperature was increased up to 70 °C. After the urea solution was added, the temperature of the mixture was raised to 80 °C. Stirring was continued, so that the total volume of the mixture, whose temperature was kept constant, was reduced to half. The resulting brown precipitate was allowed to cool at room temperature and then washed repeatedly with distilled water and ethanol. Finally, it was left to dry in an oven at 70 °C for 4 h (Fig. 1).

Nanocubes synthesis

The preparation method of NC@α-Fe_2O_3 was optimized by according to the approach of reference (Devi et al. 2021). First, two different solutions were prepared for nanocube synthesis. $FeCl_3$ was used in the first solution preparation. 3.24 g of $FeCl_3$ was added to 100 mL of distilled water and stirred for 20 min. until completely dissolved. In the second solution, you added 0.9 g of urea in 100 mL of distilled water and stirred for 20 min. Then, these two solutions were mixed at room temperature until they became homogeneous. The resulting mixture was kept in an autoclave at 135 °C for

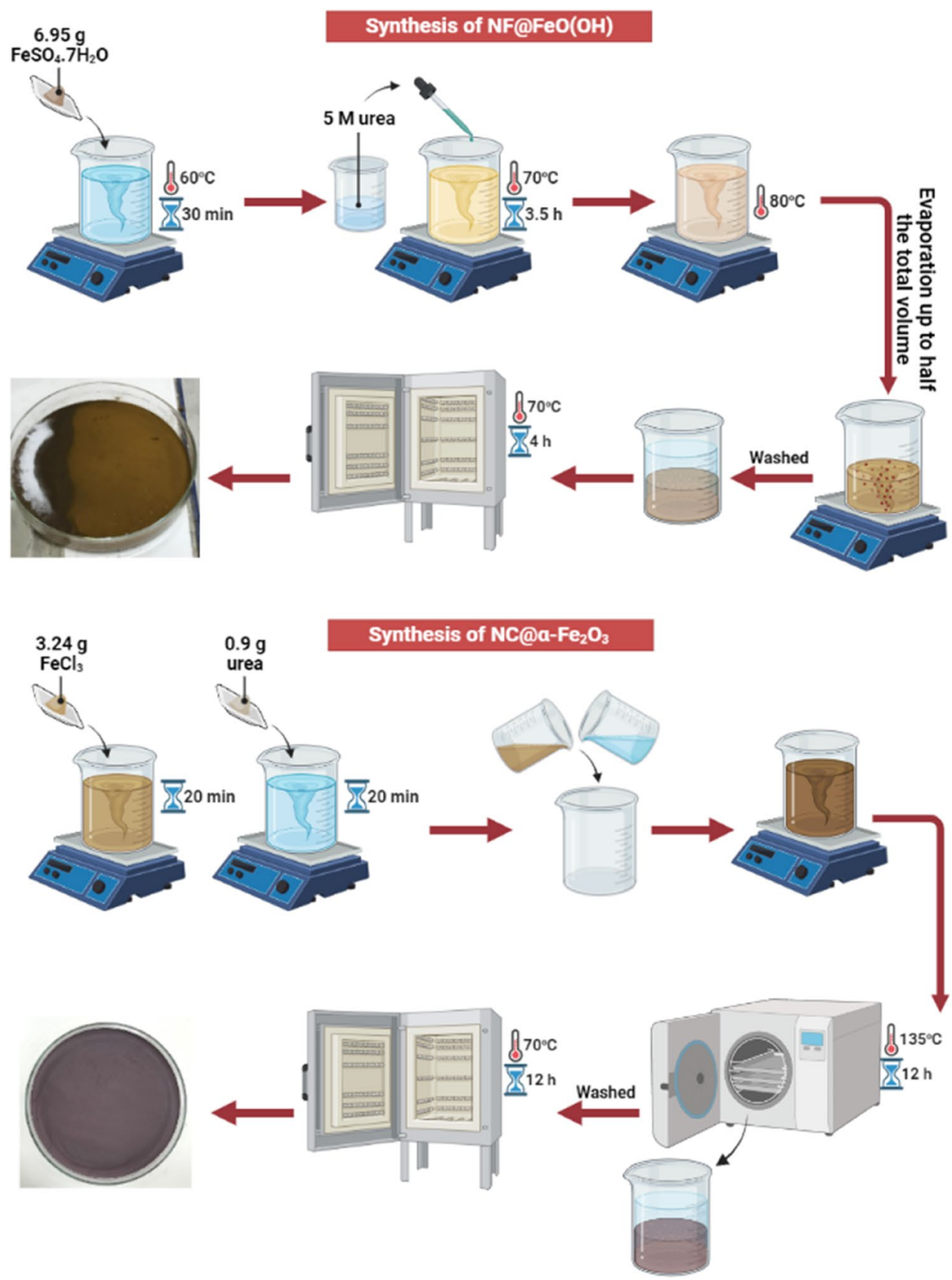

Fig. 1 Flow chart of synthesizing NF@FeO(OH) and NC@α-Fe_2O_3

12 h and allowed room temperature for cooling. After performing all the steps of the synthesis method, the top water of the dark purple precipitate was removed after the particles precipitated. The precipitate separated from the top water was thoroughly washed with distilled water. It was then dried in an oven at 70 °C overnight. The powdered material was stored in a desiccator until characterization analysis (Fig. 1).

Characterization of nanoparticles

SEM–EDX were used for the morphology and elemental composition of the synthesized nanoflowers and nanocubes. The chemical structure of the nanoparticles was determined using XRD, with 2θ scan from 10° to 90°.

Activity of NF@FeO(OH) and NC@α-Fe_2O_3 of DPPH

The DPPH free radical scavenging ability was applied to test the antioxidant capability of NF@FeO(OH) and NC@α-Fe_2O_3 and the method was performed as previously indicated by Ağırtaş et al. (2015).

DNA cleavage ability of NF@FeO(OH) and NC@α-Fe_2O_3

The impact of newly synthesized NF@FeO(OH) and NC@a-Fe2O3 on DNA molecules was investigated using *E. coli* plasmid DNA. The study was applied as previously performed by Gonca et al. (2022).

Activity of NF@FeO(OH) and NC@α-Fe_2O_3 of antimicrobial

The conventional microdilution technique was used to validate the antimicrobial ability of NF@FeO(OH) and NC@α-Fe_2O_3. The study was applied as previously performed by Gonca et al. (2022, 2021).

Bacterial viability inhibition test

Microbial cell viability inhibition study was performed to evaluate effect of newly synthesized NF@FeO(OH) and NC@α-Fe_2O_3 on the growth inhibition of *E. coli* as a goal bacterium. Cell viability study was carried out according to the study of Gonca et al. (2022). Freshly prepared *E. coli* was collected after washing with NaCl and made ready for use in the experiment by adding sterile NaCl solution (10 mL). The suspension was co-treated with NF@FeO(OH) and NC@a-Fe_2O_3 and the mixtures were incubated for 1 h. It was then diluted and injected into solid Nutrient medium before being incubated. The colonies were then enumerated and cell viability inhibition was estimated.

Biofilm inhibition activity

In this study, biofilm inhibition of newly synthesized NF@FeO(OH) and NC@α-Fe_2O3 was studied using *S. aureus* and *P. aeruginosa* bacteria, with reference to the study by Gonca et al. (2021). First of all, NF@FeO(OH) and NC@α-Fe_2O_3 were prepared at three different concentrations including 125, 250 and 500 mg/L in a 24 well plates. After that, the corresponding wells were infected with *S. aureus* and *P. aeruginosa*, and the incubation period was 72 h at 37 °C. Positive control wells were determined as wells without NF@FeO(OH) and NC@a-Fe_2O_3. The wells were emptied completely after the waiting period and thoroughly washed. The plates were kept in an oven to dry. Afterwards, the plates dried for 45 min were allowed to stand by adding crystal violet (CV) dye and were separated from the CV at the end of the time. After the biofilm had adsorbed the CV well, it was dissolved with ethanol. Measurement was performed using a spectrophotometer with an adsorbent value of 595 nm and was calculated to determine biofilm inhibition.

Results and discussion

Characterization of nanoparticles

In this study, XRD results for NF@FeO(OH) show many α-FeOOH peaks. The XRD results of the nanoflowers are given in Fig. 2. As presented in Fig. 2a, the peaks centered at 21.2°, 33.2°, 36.6° and 53.2° corresponding to the (110), (130), (111) and (221) can be indexed to the orthogonal phase of α-FeOOH, respectively (Huang et al. 2020; Hu et al. 2019). As shown in Fig. 2b, NC@α-Fe_2O_3 nanoparticle shows the presence of characteristics peaks corresponding to 24.1°, 33.1°, 35.6°, 40.8°, 49.4°, 54.05°, 62.42° and 63.9° for (102), (104), (110), (113), (024), (116), (214) and (300) planes of nanocubes α-Fe_2O_3 phase, respectively (Pan et al. 2021; Liu et al. 2019). The characteristic peaks of the XRD peaks of α-FeOOH and α-Fe_2O_3 indicate the high purity of the obtained nanoflowers and nanocubes. Peaks corresponding to both goethite and hematite components confirm the presence of α-FeOOH and α-Fe_2O_3 in the synthesized nanoparticles.

The surface morphology and shape of NF@FeO(OH) and NC@α-Fe_2O_3 were examined by SEM and are given in Fig. 3. The SEM images of NF@FeO(OH) in Fig. 3a, b shows that it has many flower-like morphologies and that they are evenly distributed. The iron oxide-hydroxide particle was found to have flower-like morphology and Fig. 3a, b support the morphological structure. Many blocks occur together in the SEM picture of NC@-Fe_2O_3, as illustrated in Fig. 3c. It clearly shows the morphology of the blocks and reveals their cubic shape with good uniformity. The particles

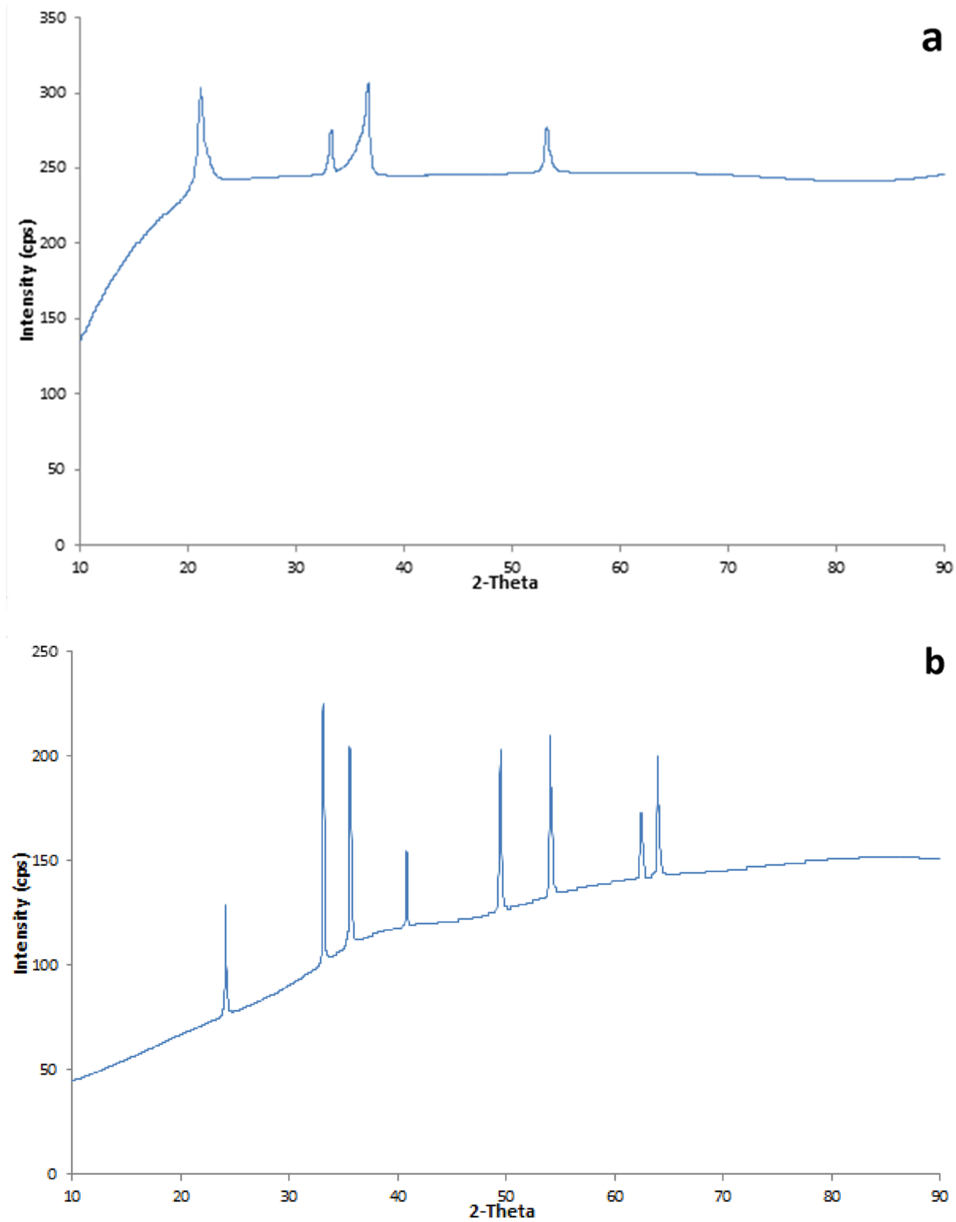

Fig. 2 XRD patterns of nanoparticules; **a** NF@FeO(OH), **b** NC@α-Fe_2O_3

size of diameters of the particles is indicated as 850 nm in Fig. 3d.

The SEM–EDX results of the synthesized nanoparticles are shown in Fig. 4. Figure 4a shows the presence of peaks corresponding to C (9.67% w/w), N (5.81% w/w), O (32.2% w/w) and Fe (%52.32) according to the EDX spectra of NF@FeO(OH). The EDX peaks support the XRD results and indicate the purity of the synthesized nanoflower. EDX results for NC@α-Fe_2O_3 are given in Fig. 4b. The three obvious peaks of Fe were seen in accord with C, O and Cl, respectively. The weights of Fe, C, O and Cl elements are %7.58, %17.74, %0.79 and %73.79, respectively. The carbon and nitrogen elements probably originate from the urea used during the synthesis of the nanoparticles. In addition, it is thought that the Cl in the EDX peak of the nanocube comes from $FeCl_3$.

DPPH radical scavenging activity

Studies have revealed that substances with antioxidant activity have an important function in the prevention of cataracts, cancer, cardiovascular and many other diseases that are thought to be caused by oxidative stress (Niki 2010). As a result of these factors, the need for alternative natural or synthetic antioxidant molecules is growing by the day. In this investigation, the DPPH radical scavenging ability of both chemically synthesized of iron oxide nanoparticles were carried out by DPPH procedure. The data

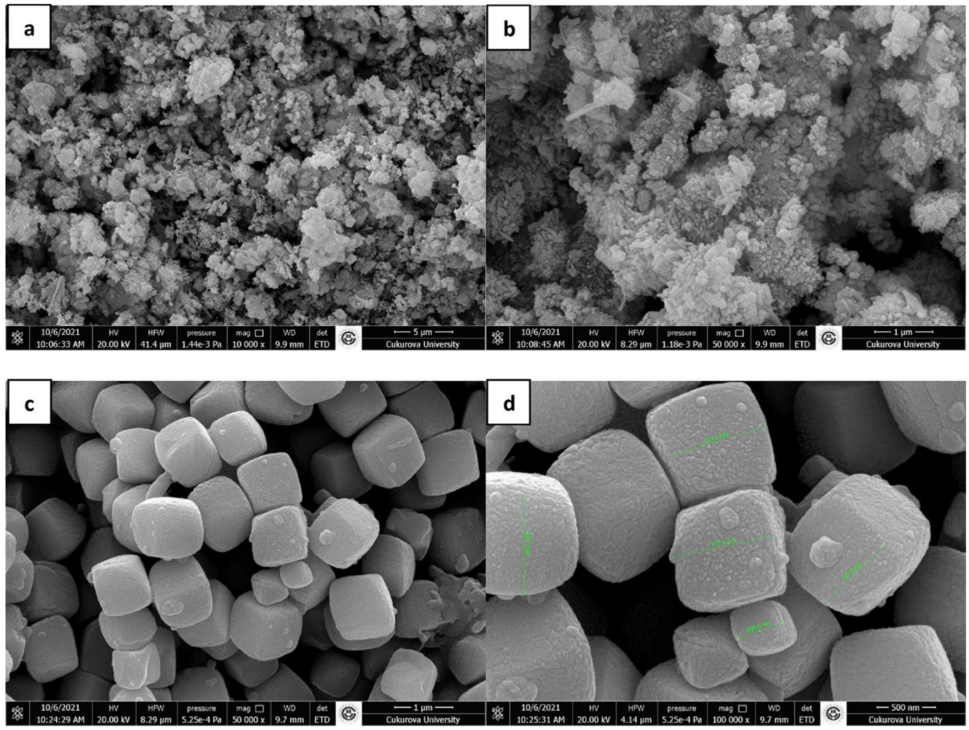

Fig. 3 **a**, **b** SEM image of NF@FeO(OH) and **c**, **d** SEM image of NC@α-Fe_2O_3

are represented in Fig. 5. It is obviously seen from Fig. 5 that by increase in amount of both iron oxide nanoparticles the range of scavenging activity also increased. It was determined that the DPPH radical inhibition was found as 17.83% for NF@FeO(OH) and 27.10% for NC@α-Fe_2O_3 at 25 mg/L. DPPH scavenging activity improved from 36.67% to 57.39% and from 42.32% to 60.00% when the concentration of NF@FeO(OH) and NC@-Fe_2O_3 increased from 50 to 100 mg/L, respectively. According to these results, the highest DPPH scavenging abilities of NF@FeO(OH) and NC@α-Fe_2O_3 were 63.48% and 71.30% at concentration of 200 mg/L, respectively. Our results showed that the new synthesized NF@FeO(OH) and NC@α-Fe_2O_3 can donate proton or electron which in turn inhibits the DPPH free radicals and also NC@α-Fe_2O_3 showed more effective radical inhibition activity than NF@FeO(OH). Khan et al. (2021) synthesized ZnO nanoflowers. They evaluated the in vitro DPPH inhibitory activity of ZnO nanoflower. They discovered that DPPH inhibitory action was concentration dependent, with the maximum DPPH radical scavenging ability of 60% at 5000 mg/L, confirming the results of the characterization analyses. Patra and Baek (2017) reported that they synthesized two different Fe-NPs and investigated their DPPH scavenging ability. The outer leaves of Chinese cabbage derivated-FeNP and maize silky hairs derivated-FeNP also showed 27.30% and 26.98% at 100 μg/mL. Mohamed et al. (2021) reported that they used a green and chemical technique to create iron oxide nanoparticles. They investigated the iron oxide nanoparticles (IONPs)' antioxidant properties following the synthesis method. They found that chemically (Chem-IONPs), aloe Vera (AV-IONPs), curcumin (Cur-IONPs) and green tea (GT-IONPs) exhibited 26%, 45%, 58%, and 33% DPPH radical scavenging activity at 5000 mg/L. Our results showed higher DPPH inhibition ability with their findings. Due to their strong antioxidant activity, the NF@FeO(OH) and NC@α-Fe_2O_3 appear to be the most suitable candidates.

DNA cleavage ability

The importance of this molecule in cells is well-known, since even the smallest change in the DNA molecule can have a significant effect on the cell. As a result, it is a significant anticancer and antibacterial target molecule. The effects of synthesized NF@FeO(OH) and NC@α-Fe_2O_3 on DNA were investigated in this work. As a result, plasmid DNA was chosen as the target molecule, and DNA damage was detected using the agarose gel electrophoresis technique. Figure S1 depicts all of the acquired results. As shown in Fig. S1, newly synthesized NF@FeO(OH) and NC@-Fe_2O_3 shown good DNA nuclease activity, and it was discovered that NF@FeO(OH) and NC@-Fe_2O_3 totally degraded DNA into its nucleotides. When Form I, the super-helical structure of plasmid DNA, turns into an open circular form with damage to DNA, it is called Form II. The linear structure formed as a result of the damage in both yarns is known as Form III observed between Form I and Form II. Form I, one of the three bands formed as

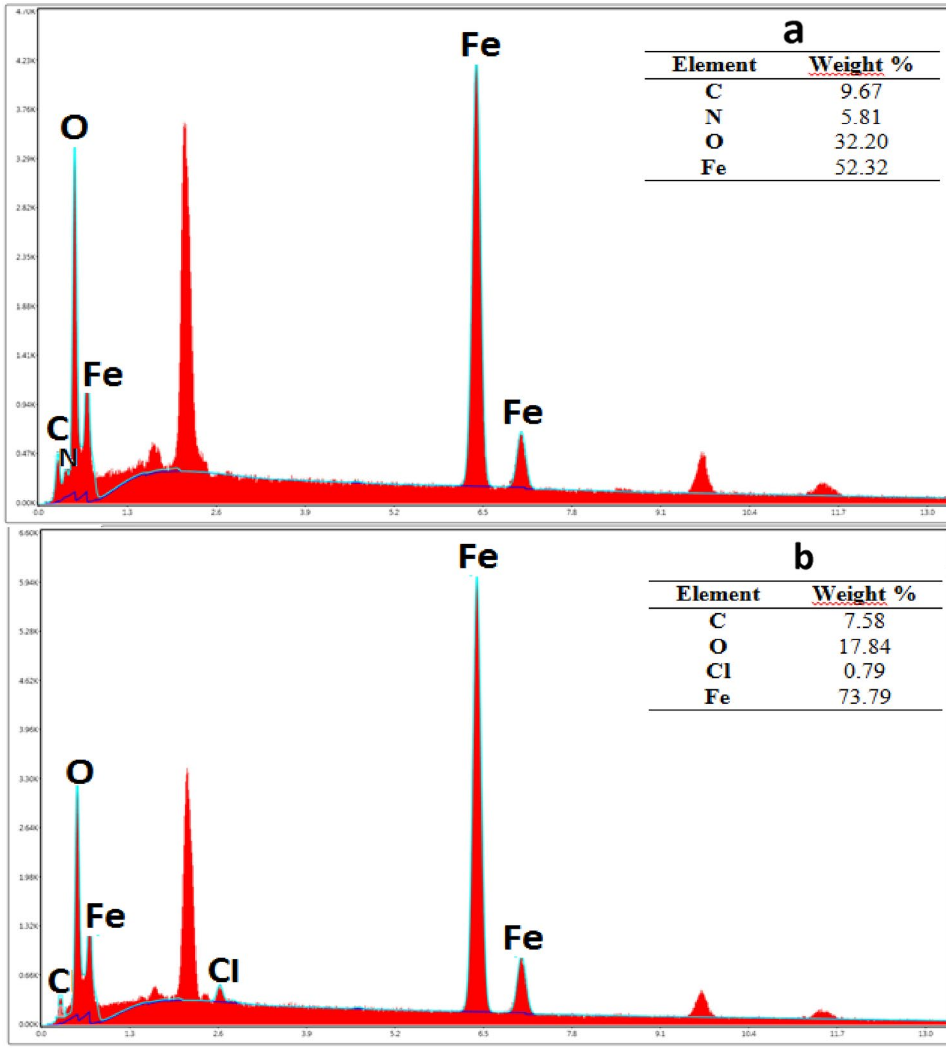

Fig. 4 EDX spectra of **a** NF@FeO(OH); **b** NC@α-Fe_2O_3 nanoparticles

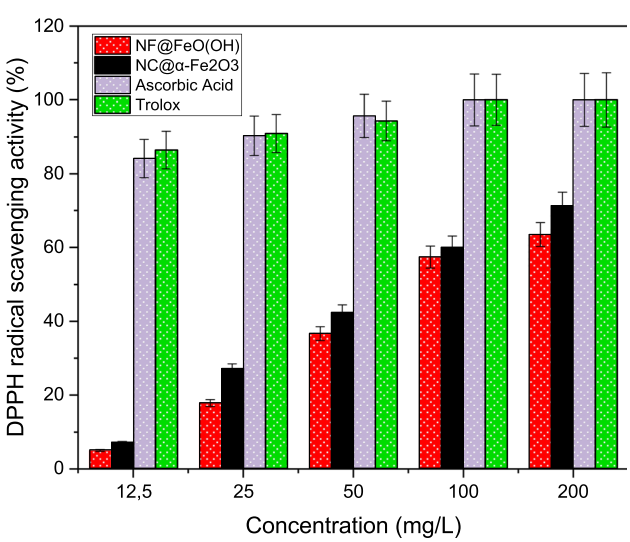

Fig. 5 Comparison of DPPH scavenging efficiency of NF@FeO(OH) and NC@α-Fe_2O_3 with other chemicals

a result of agarose gel electrophoresis, moves faster than Form II and Form III. This is due to the large load density and low volume (Mansour and Ragab 2019). According to Sohrabijam et al. (2017), they investigated the effect of chitosan coated superparamagnetic nanoparticles on DNA molecules. Their research found that when DNA interacted with different concentrations of chitosan coated superparamagnetic iron oxide nanoparticles, its conformation altered. Asadi et al. (2017) noticed that they studied they investigated the DNA interaction of chitosan-coated magnetic nanoparticles (CS-MNPs) with pBluescript II KS (+) plasmid DNA and it was determined that CS-MNPs demonstrated DNA cleavage ability. These results support our findings. According to these results, the new synthesized of NF@FeO(OH) and NC@α-Fe_2O_3 can be utilized in drug industries as anti-cancer and antimicrobial agents after further investigations.

Fig. 6 Biofilm inhibition of *S. aureus* for NF@FeO(OH) and NC@α-Fe_2O_3

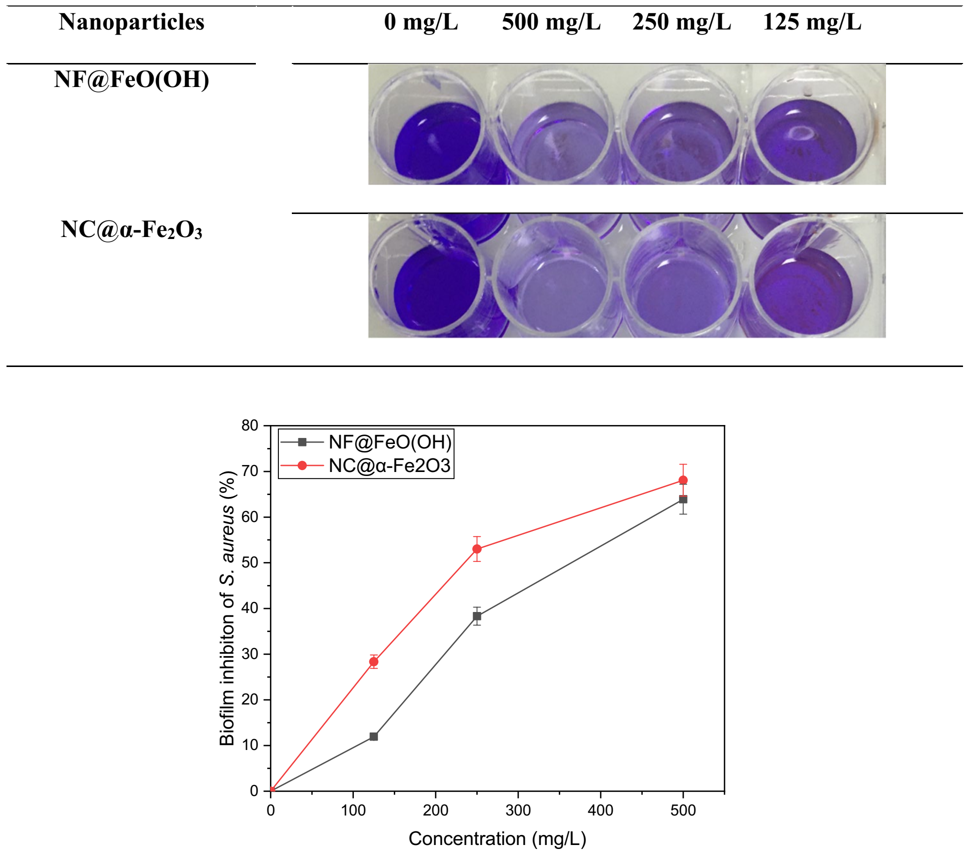

Antimicrobial activity

Nanoparticles (NPs) have been extensively studied for their antimicrobial activity, so that they can act as a possible agent for designing drugs for therapeutic studies (Ansari et al. 2017). For that reason, we investigated the effect of new synthesized and characterized NF@FeO(OH) and NC@α-Fe_2O_3 on antimicrobial activity against test microorganisms using micro-dilution assay. The results are represented in Table S1. MIC values of NF@FeO(OH) were found as 256 mg/L for *E. coli*, *C. parapisilosis* and *P. aeruginosa,* 128 mg/L for *L. pneumophila, E. hirae,* and *S. aureus, C. tropicalis* and 64 mg/L for *E. fecalis*. On the other hand, MIC values of NC@α-Fe_2O_3 were determined as 256 mg/L for *E. coli* and *C. tropicalis,* 128 mg/L for *P. aeruginosa*, *L. pneumophila*, *E. hirae, S. aureus* and *C. parapisilosis* and 32 mg/L for *E. fecalis*. *E. fecalis* was found to be the microbe that responded to the newly synthesized NF@FeO(OH) and NC@-Fe_2O_3 the most, as indicated by the findings. There have not been enough antimicrobial studies on NF@FeO(OH) and especially NC@α-Fe_2O_3 although there have been antimicrobial studies on different metal nanoparticles and different types of nanoparticles in the literature. Ashkarran et al. (2013) studied the antimicrobial activity of different geometries of silver nanostructures with including triangle, cube, sphere and wire which synthesized using solution-phase process. It was determined that all different geometries of silver nanostructures displayed antimicrobial effect. These cubic, wiry, spherical, and triangular NPs also showed the highest antimicrobial activity against *S. aureus* among the test microorganisms. Krishnamoorthy et al. (2014) reported that they synthesized new cerium oxides nanocubes and they also investigated the antimicrobial activity of cerium oxides nanocubes. It was found that cerium oxides nanocubes displayed significant antimicrobial activity against to test microorganisms. Mohamed et al. (2020) used several microbial strains to perform antibacterial tests on the produced nanoparticles to investigate the antibacterial characteristics of green generated Fe_2O_3 NPs. Fe_2O_3 nanoparticles were shown to be antibacterial against *B. subtilis*, *P. aeruginosa*, and *S. epidermidis*. The nanoparticles have demonstrated their antimicrobial potential, the effects of ferric ions by causing changes in the conformational structures of microbial DNA and proteins. Thus, it leads to a decrease in microbial cell numbers. In addition, the generation of reactive oxygen species is one of the possible mechanisms by which iron oxide nanoparticles show antimicrobial activity (Ansari et al. 2017). In addition to these, difference in antimicrobial

Fig. 7 Biofilm inhibition of *P. aeruginosa* for NF@FeO(OH) and NC@α-Fe_2O_3

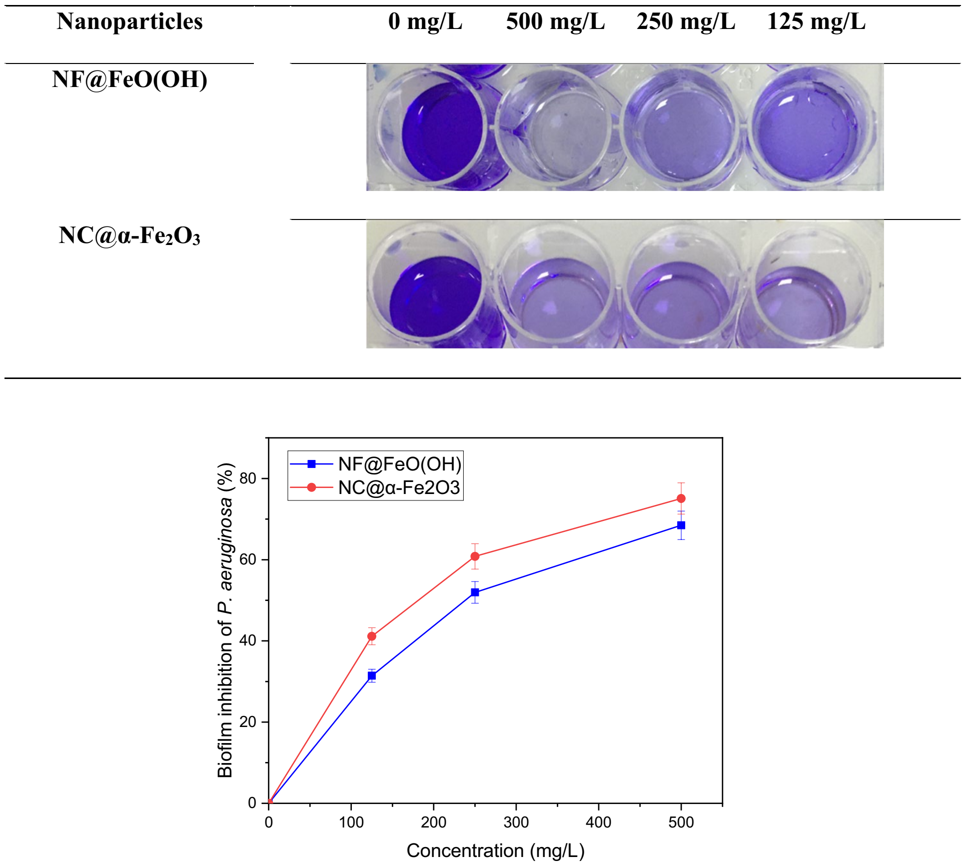

activity results can be explained by the physicochemical and morphological characteristics, such as positive surface charge, shape, size of the NPs (Ashkarran et al. 2013). These similar antimicrobial mechanisms may have shown efficacy against the tested microorganisms in this study as well when using NF@FeO(OH) and NC@α-Fe_2O_3. As a result, NF@FeO(OH) and NC@α-Fe_2O_3 need to be developed with further studies to be used as antimicrobial agents in the pharmaceutical industry.

Biofilm inhibition activity

Biofilm, which is a microbial life form frequently encountered in the natural environment, can be defined as a micro-ecosystem formed by various microbial species to be protected from environmental factors and to stay in a suitable environment for their vital activities (Krishnamoorthy et al. 2014). The biofilm structure that microorganisms form after they attach irreversibly to a living or non-living interface through organic exopolysaccharide structures they produce provides advantages for the microorganism in terms of escape from host defense and resistance to antibiotics (Marcinkiewicz et al. 2013; Høiby et al. 2011). Microbial biofilm formation on surfaces has been investigated for many years and is now accepted as one of the major factors in many bacterial infections with chronic tissue damage (Høiby et al. 2011). Infections that develop as a result of biofilms formed on different medical devices and biomaterials such as intravenous catheters, implants, heart valves, and contact lenses cause serious therapeutic problems in patients (Lindsay and Holy 2006). In this study, *P. aeruginosa* and *S. aureus* were used as the biofilm-forming bacteria to examine the ability of NF@FeO(OH) and NC@α-Fe_2O_3 to suppress the growth of biofilms. Figures 6 and 7 were illustrated the biofilm inhibition of *S. aureus* and *P. aeruginosa*. It was discovered that the biofilm inhibition ability of NF@FeO(OH) and NC@α-Fe_2O_3 was concentration-dependent. At all tested dosages, NC@α-Fe_2O_3 shown superior biofilm suppression efficacy than NF@FeO(OH) for both test species. When used at 125 mg/L, NF@FeO(OH) and NC@-Fe2O3 had biofilm inhibition activities against *P. aeruginosa* and *S. aureus* of 31.43%, 41.14%, and 11.94%, 28.35%, respectively. The concentrations of NF@FeO(OH) and NC@α-Fe_2O_3 were increased from 250 to 500 mg/L, the biofilm inhibition activity of *P. aeruginosa* increased from 51.96% to 68.48% and from 60.82% to 75.07%, respectively, and of *S. aureus* increased from 38.30% to 63.91% and from 53.02% to 68.06%, respectively. Selim et al. (2020) reported that they decorated graphene oxide with Cu_2O nanocube composite. They also investigated the antibiofilm activity

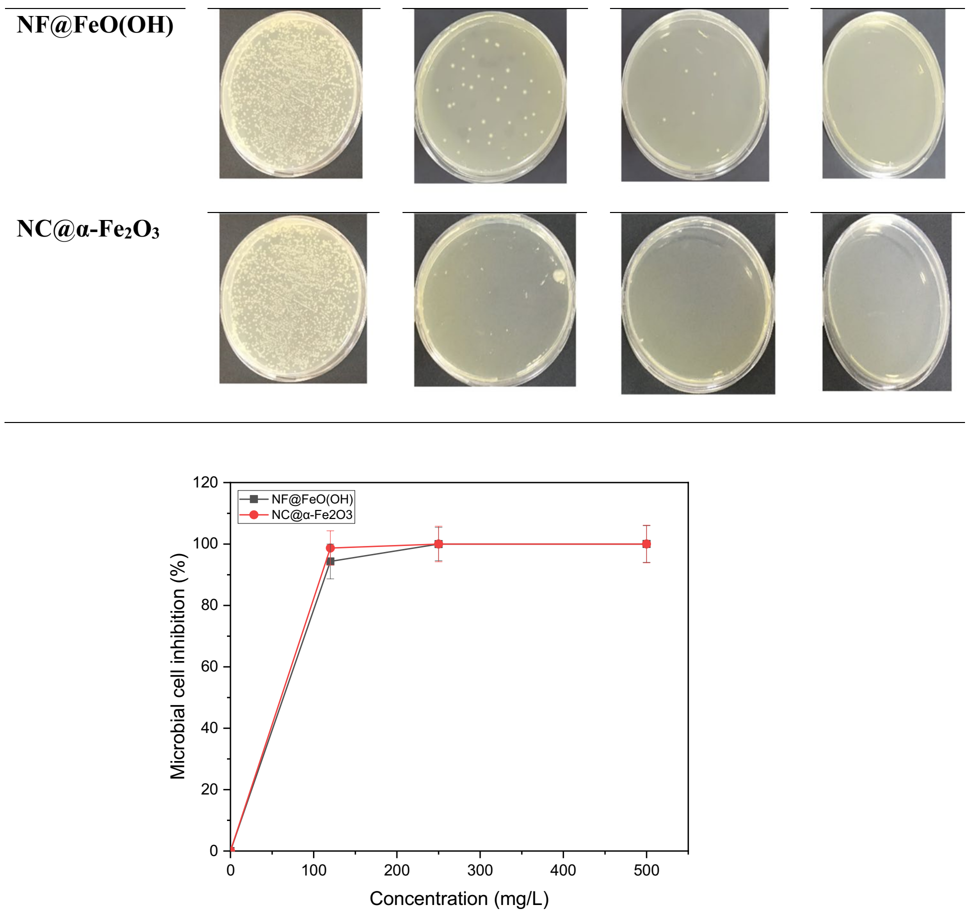

Fig. 8 Microbial cell inhibition of *E. coli* for NF@FeO(OH) and NC@α-Fe_2O_3

and it was found that the biofilm activity of *B. subtilis*, *P. aeruginosa*, and *E. coli* was significantly inhibited. Khalid et al. (2019) synthesized rhamnolipid-coated iron oxide and silver (Ag) NPs. They stated that they developed an easy process for the synthesis method used in their study. They also investigated the effect of biofilm inhibition produced NPs on bacteria using *P. aeruginosa* and *S. aureus* bacteria. In addition, it was determined that these NPs exhibited significant anti-biofilm activity against both microorganisms. It may be concluded that newly synthesized NF@FeO(OH) and NC@-Fe_2O_3 could be used as a potent alternative in medical applications to reduce infection severity through biofilm inhibition.

Microbial cell viability

Analyzes were carried out in our study to test the inhibition activity of microbial cell viability of newly synthesized NF@FeO(OH) and NC@α-Fe_2O_3. The results are presented in Fig. 8. These findings led to the conclusion that the newly created nanoparticles effectively inhibited the development of *E. coli*. New synthesized NF@FeO(OH) and NC@α-Fe_2O_3 growth inhibited the *E. coli* as 94.32% and 98.66% at 125 mg/L and 99.98% and 100% at 250 mg/L, respectively, in Fig. 8. It was also found that both new synthesized iron NPs demonstrated 100% bacterial cell inhibition at 500 mg/L.

Janani et al. (2021) used bacterial strains such as *E. coli* and *Bacillus subtilis* to test the antibacterial activity of FeV_2O_4 NCs. Antibacterial ability of the NCs against to *E. coli* and *B. subtilis* was investigated by exposing the microbial strains to NCs of between the concentration of 0.1–50 mg/L. An increase in bacterial growth inhibition was seen with increasing concentration of NCs, where high sensitivity was demonstrated by *E. coli*. The negatively charged microbial cell surface leads to interspersed electron transfer between cellular transmembranes. This situation causes various stresses in cells and as a result, they produce reactive oxygen species (ROS). These ROS can be caused cell detriment break peptide bonds of proteins or protein–protein cross-links (Selim et al. 2020). According to these results, in the pharmaceutical sector newly synthesized iron nanoparticles of various forms can be utilized as antibacterial agents. Güven et al. (2022) investigated the antibacterial effect on gram-positive and gram-negative bacteria with the copper-containing material obtained from cherry stalk. They determined different MIC values for bacteria, such as *P. aeruginosa* (10 mg/mL), *E. coli* (2.5 mg/mL) and *E. fecalis* (2.5 mg/mL). They stated that by adding different amounts of copper into the composite material, the functionality of the synthesized material should be increased for its use in the biomedical field. In another study, Lee et al. (2020) investigated the antibacterial properties (MIC value: 10 mg/mL) of the glucose oxidase-containing nanoflower material against *E. coli* in their study. They obtained more MIC values compared to our study.

Conclusion

In this study, two different types of iron nanoparticles were prepared. Characterization and morphology analyzes of the synthesized nanoparticles were performed. When the SEM images were examined, it was determined that NF@FeO(OH) had a flower-like morphology and it was a goethite (α-FeOOH) type of iron oxide according to both XRD and EDX results. NC@α-Fe_2O_3, which was found to have a cube-shaped structure in the SEM image, was found to contain hematite (α-Fe_2O_3) type iron oxide in XRD and EDX results. One of the aims of this study is to test various biological activities of newly synthesized NF@FeO(OH) and NC@α-Fe_2O_3. The antioxidant, antibacterial, biofilm inhibition, DNA cleavage, and microbial cell viability suppression effects of these iron nanoparticles were investigated for this aim. Using NF@FeO(OH), MIC values were determined as 256 mg/L for *E. coli, P. aeruginosa* and *C. parapsilosis*. While it was 128 mg/L for *L. pneumophila, E. hirae, S. aureus* and *C. tropicalis*, it was determined as 64 mg/L for *E. fecalis*. In NC@α-Fe_2O_3 material, it was determined as 256 mg/L for *E. coli* and *C. tropicalis*, and 128 mg/L for *P. aeruginosa, L. pneumophila, E. hirae, S. aureus* and *C. parapsilosis*. In addition, 32 mg/L was accepted as the appropriate value for *E. fecalis*. NF@FeO(OH) and NC@α-Fe_2O_3 growth inhibited the *E. coli* as 94.32% and 98.66% at 125 mg/L and 99.98% and 100% at 250 mg/L, respectively. Based on these findings, we believe that the newly synthesized chemicals can be employed for a variety of applications in the pharmaceutical business after passing numerous toxicological tests.

Supplementary Information The online version contains supplementary material available at https://doi.org/10.1007/s13204-023-02822-5.

Data availability The data that support the findings of this study are available from the corresponding author (N.D), upon reasonable request.

Declarations

Conflict of interest The author declare that they have no known competing financial interests or personal relationships that could have appeared to influence the work reported in this paper.

References

Ağırtaş MS, Karataş C, Özdemir S (2015) Synthesis of some metallophthalocyanines with dimethyl 5-(phenoxy)-isophthalate substituents and evaluation of their antioxidant-antibacterial activities. Spectrochim Acta Part A Mol Biomol Spectrosc 135:20–24

Alhallak K, Sun J, Wasden K, Guenthner N, O'Neal J, Muz B et al (2021) Nanoparticle T-cell engagers as a modular platform for cancer immunotherapy. Leukemia. https://doi.org/10.1038/s41375-021-01127-2

Ansari SA, Oves M, Satar R, Khan A, Ahmad SI, Jafri MA et al (2017) Antibacterial activity of iron oxide nanoparticles synthesized by co-precipitation technology against Bacillus cereus and Klebsiella pneumoniae. Pol J Chem Technol 19(4):110–115

Asadi Z, Nasrollahi N, Karbalaei-Heidari H, Eigner V, Dusek M, Mobaraki N, Pournejati R (2017) Investigation of the complex structure, comparative DNA-binding and DNA cleavage of two water-soluble mono-nuclear lanthanum (III) complexes and cytotoxic activity of chitosan-coated magnetic nanoparticles as drug delivery for the complexes. Spectrochim Acta Part A Mol Biomol Spectrosc 178:125–135

Ashkarran AA, Estakhri S, Nezhad MRH, Eshghi S (2013) Controlling the geometry of silver nanostructures for biological applications. Phys Procedia 40:76–83

Aslanidis E, Skotadis E, Tsoukalas D (2021) Simulation tool for predicting and optimizing the performance of nanoparticle based strain sensors. Nanotechnology 32(27):275501

Cabana S, Curcio A, Michel A, Wilhelm C, Abou-Hassan A (2020) Iron oxide mediated photothermal therapy in the second biological window: a comparative study between magnetite/maghemite nanospheres and nanoflowers. Nanomaterials 10(8):1548

Cevaal PM, Ali A, Czuba-Wojnilowicz E, Symons J, Lewin SR, Cortez-Jugo C, Caruso F (2021) In vivo T cell-targeting nanoparticle drug delivery systems: considerations for rational design. ACS Nano 15(3):3736–3753

Clark BD, Jacobson CR, Lou M, Renard D, Wu G, Bursi L et al (2019) Aluminum nanocubes have sharp corners. ACS Nano 13(8):9682–9691

Devi S, Sharma V, Chahal S, Goel P, Singh S, Kumar A, Kumar P (2021) Phase transformation and structural evolution in iron oxide nanostructures. Mater Sci Eng B 272:115329

Duan JJ, Zhang RL, Feng JJ, Zhang L, Zhang QL, Wang AJ (2021) Facile synthesis of nanoflower-like phosphorus-doped Ni_3S_2/$CoFe_2O_4$ arrays on nickel foam as a superior electrocatalyst for efficient oxygen evolution reaction. J Colloid Interface Sci 581:774–782

Ekata D, Salunkhe KA, Shedage AR (2020) Review on nanoflowers. Curr Trends Pharmacy Pharmac Chem 2:8–20

Ekennia AC, Uduagwu DN, Nwaji NN, Oje OO, Emma-Uba CO, Mgbii SI et al (2021) Green synthesis of biogenic zinc oxide nanoflower as dual agent for photodegradation of an organic dye and tyrosinase inhibitor. J Inorg Organomet Polym Mater 31(2):886–897

El-Shafai NM, Beltagi AM, Ibrahim MM, Ramadan MS, El-Mehasseb I (2021) Enhancement of the photocurrent and electrochemical properties of the modified nanohybrid composite membrane of cellulose/graphene oxide with magnesium oxide nanoparticle

(GO@ CMC. MgO) for photocatalytic antifouling and supercapacitors applications. Electrochim Acta 392:138989

Gabrielyan L, Badalyan H, Gevorgyan V, Trchounian A (2020) Comparable antibacterial effects and action mechanisms of silver and iron oxide nanoparticles on *Escherichia coli* and *Salmonella typhimurium*. Sci Rep 10(1):1–12

Gonca S, Arslan H, Isik Z, Özdemir S, Dizge N (2021) The surface modification of ultrafiltration membrane with silver nanoparticles using *Verbascum thapsus* leaf extract using green synthesis phenomena. Surf Interfaces 26:1–11

Gonca S, Ozidemir S, Isik Z, M'barek I, Shaik F, Dizge N (2022) Synthesis of silver nanoparticles from red and green parts of the pistachio hulls and their various in-vitro biological activities. Food Chem Toxicol 165:1–10

Güven OC, Kar M, Koca FD (2022) Synthesis of cherry stalk extract based organic@inorganic hybrid nanoflowers as a novel fenton reagent: evaluation of their antioxidant, catalytic, and antimicrobial activities. J Inorg Organomet Polym Mater 32(3):1026–1032

Harris J, Silk R, Smith M, Dong Y, Chen WT, Waterhouse GI (2020) Hierarchical TiO_2 nanoflower photocatalysts with remarkable activity for aqueous methylene blue photo-oxidation. ACS Omega 5(30):18919–18934

Høiby N, Ciofu O, Johansen HK, Song ZJ, Moser C, Jensen PØ et al (2011) The clinical impact of bacterial biofilms. Int J Oral Sci 3(2):55–65. https://doi.org/10.4248/IJOS11026

Hu Z, Ai Y, Liu L, Zhou J, Zhang G, Liu H et al (2019) Hydroxyl assisted rhodium catalyst supported on goethite nanoflower for chemoselective catalytic transfer hydrogenation of fully converted nitrostyrenes. Adv Synth Catal 361(13):3146–3154

Hu X, Liu S, Wang Y, Huang X, Jiang J, Cong H et al (2021) Hierarchical $CuCo_2O_4$@ CoS-Cu/Co-MOF core-shell nanoflower derived from copper/cobalt bimetallic metal–organic frameworks for supercapacitors. J Colloid Interface Sci 600:72–82

Huang S, Zhang Q, Liu P, Ma S, Xie B, Yang K, Zhao Y (2020) Novel up-conversion carbon quantum dots/α-FeOOH nanohybrids eliminate tetracycline and its related drug resistance in visible-light responsive Fenton system. Appl Catal B 263:118336

Janani B, Swetha S, Syed A, Elgorban AM, Zaghloul NS, Thomas AM et al (2021) Spinel FeV_2O_4 coupling on nanocube-like Bi_2O_3 for high performance white light photocatalysis and antibacterial applications. J Alloy Compd 887:161432

Karthika A (2021) Biocompatible iron and copper incorporated nanohydroxyapatite coating for biomedical implant applications. Mater Today Proc 51:1754–1759

Khalid HF, Tehseen B, Sarwar Y, Hussain SZ, Khan WS, Raza ZA et al (2019) Biosurfactant coated silver and iron oxide nanoparticles with enhanced anti-biofilm and anti-adhesive properties. J Hazard Mater 364:441–448

Khan FU, Khan ZUH, Ma J, Khan AU, Sohail M, Chen Y et al (2021) An Astragalus membranaceus based eco-friendly biomimetic synthesis approach of ZnO nanoflowers with an excellent antibacterial, antioxidant and electrochemical sensing effect. Mater Sci Eng C 118:111432

Krishnamoorthy K, Veerapandian M, Zhang LH, Yun K, Kim SJ (2014) Surface chemistry of cerium oxide nanocubes: toxicity against pathogenic bacteria and their mechanistic study. J Ind Eng Chem 20(5):3513–3517

Kumar PM, Mylsamy K, Prakash KB, Nithish M, Anandkumar R (2021) Investigating thermal properties of Nanoparticle Dispersed Paraffin (NDP) as phase change material for thermal energy storage. Mater Today Proc 45:745–750

Lee I, Cheon HJ, Adhikari MD, Tran TD, Yeon KM, Kim MI, Kim J (2020) Glucose oxidase-copper hybrid nanoflowers embedded with magnetic nanoparticles as an effective antibacterial agent. Int J Biol Macromol 155:1520–1531

Lei H, Wu M, Liu Y, Mo F, Chen J, Ji S et al (2021) Built-in piezoelectric field improved photocatalytic performance of nanoflower-like Bi2WO6 using low-power white LEDs. Chin Chem Lett 32(7):2317–2321

Li J, Guan X, Zhang WX (2021) Architectural genesis of metal(loid)s with ıron nanoparticle in water. Environ Sci Technol. https://doi.org/10.1021/acs.est.1c02458

Lindsay D, Von Holy A (2006) Bacterial biofilms within the clinical setting: what healthcare professionals should know. J Hosp Infect 64(4):313–325. https://doi.org/10.1016/j.jhin.2006.06.028

Liu A, Zhang C, Zhu Y, Li K, Huang J, Du Y, Yang P (2019) Sn-doped hematite modified by CaMn2O4 nanowire with high donor density and enhanced conductivity for photocatalytic water oxidation. J Colloid Interface Sci 535:408–414

Liu Z, Mukherjee M, Wu Y, Huang Q, Cai P (2021) Increased particle size of goethite enhances the antibacterial effect on human pathogen *Escherichia coli* O157: H7: a raman spectroscopic study. J Hazard Mater 405:124174

Mansour AM, Ragab MS (2019) DNA/lysozyme binding propensity and nuclease properties of benzimidazole/2, 2′-bipyridine based binuclear ternary transition metal complexes. RSC Adv 9(53):30879–30887

Marcinkiewicz J, Strus M, Pasich E (2013) Antibiotic resistance: a "dark side" of biofilm associated chronic infections. Polskie Archiwum Medycyny Wewnętrznej=polish Archives of Internal Medicine 123(6):309–313

Martín-Moreno A, Jiménez Blanco JL, Mosher J, Swanson DR, García Fernández JM, Sharma A et al (2020) Nanoparticle-delivered HIV peptides to dendritic cells a promising approach to generate a therapeutic vaccine. Pharmaceutics 12(7):656

Mimura KI, Kato K (2020) High refractive index and dielectric properties of $BaTiO_3$ nanocube/polymer composite films. J Nanopart Res 22(8):1–9

Mohamed HEA, Afridi S, Khalil AT, Ali M, Zohra T, Salman M et al (2020) Bio-redox potential of Hyphaene thebaica in biofabrication of ultrafine maghemite phase iron oxide nanoparticles (Fe_2O_3 NPs) for therapeutic applications. Mater Sci Eng C 112:110890

Mohamed N, Hessen OE, Mohammed HS (2021) Thermal stability, paramagnetic properties, morphology and antioxidant activity of iron oxide nanoparticles synthesized by chemical and green methods. Inorg Chem Commun 128:108572

Mohammad M, Ahmadpoor F, Shojaosadati SA (2020) Mussel-inspired magnetic nanoflowers as an effective nanozyme and antimicrobial agent for biosensing and catalytic reduction of organic dyes. ACS Omega 5(30):18766–18777

Niki E (2010) Assessment of antioxidant capacity in vitro and in vivo. Free Radical Biol Med 49(4):503–515

Niu W, Sun J, Zhang L, Cao F (2021) The enhanced removal of highly toxic Cr (VI) by the synergy of uniform fiber ball loaded with $Fe(OH)_3$ and oxalate acid. Chemosphere 262:127806

Okejiri F, Zhang Z, Liu J, Liu M, Yang S, Dai S (2020) Room temperature synthesis of high entropy perovskite oxide nanoparticle catalysts through ultrasonication based method. Chemsuschem 13(1):111–115

Ouyang B, Poon W, Zhang YN, Lin ZP, Kingston BR, Tavares AJ et al (2020) The dose threshold for nanoparticle tumour delivery. Nat Mater 19(12):1362–1371

Pan W, Zhang Y, Yu S, Liu X, Zhang D (2021) Hydrogen sulfide gas sensing properties of metal organic framework-derived α-Fe_2O_3 hollow nanospheres decorated with $MoSe_2$ nanoflowers. Sens Actuators B Chem 344:130221

Patra JK, Baek KH (2017) Green biosynthesis of magnetic iron oxide (Fe3O4) nanoparticles using the aqueous extracts of food processing wastes under photo-catalyzed condition and

investigation of their antimicrobial and antioxidant activity. J Photochem Photobiol B 173:291–300
Pham TT, Ngo HH, Nguyen MK (2020) Removal of As (V) from the aqueous solution by a modified granular ferric hydroxide adsorbent. Sci Total Environ 706:135947
Pramanik A, Gao Y, Patibandla S, Mitra D, McCandless MG, Fassero LA et al (2021) Aptamer conjugated gold nanostar-based distance-dependent nanoparticle surface energy transfer spectroscopy for ultrasensitive detection and ınactivation of corona virus. J Phys Chem Lett 12(8):2166–2171
Puri N, Gupta A, Mishra A (2021) Recent advances on nano-adsorbents and nanomembranes for the remediation of water. J Clean Prod 322:129051
Rahmati Z, Roushani M, Hosseini H, Choobin H (2021) Electrochemical immunosensor with Cu_2O nanocube coating for detection of SARS-CoV-2 spike protein. Microchim Acta 188(3):1–9
Raul PK, Devi RR, UmLong IM, Thakur AJ, Banerjee S, Veer V (2014) Iron oxide hydroxide nanoflower assisted removal of arsenic from water. Mater Res Bull 49:360–368
Seil JT, Webster TJ (2012) Antimicrobial applications of nanotechnology: methods and literature. Int J Nanomed 7:2767
Selim MS, Samak NA, Hao Z, Xing J (2020) Facile design of reduced graphene oxide decorated with Cu_2O nanocube composite as antibiofilm active material. Mater Chem Phys 239:122300
Shahabadi N, Zendehcheshm S, Khademi F, Rashidi K, Chehri K (2021) Green synthesis of Chloroxine-conjugated silver nanoflowers: promising antimicrobial activity and in vivo cutaneous wound healing effects. J Environ Chem Eng 9(3):105215
Sharma P, Pandey V, Sharma MMM, Patra A, Singh B, Mehta S, Husen A (2021) A review on biosensors and nanosensors application in agroecosystems. Nanoscale Res Lett 16(1):1–24
Sohrabijam Z, Saeidifar M, Zamanian A (2017) Enhancement of magnetofection efficiency using chitosan coated superparamagnetic iron oxide nanoparticles and calf thymus DNA. Colloids Surf B Biointerfaces 152:169–175
Subramani IG, Perumal V, Gopinath SC, Fhan KS, Mohamed NM (2021) Organic-inorganic hybrid nanoflower production and analytical utilization: fundamental to cutting-edge technologies. Crit Rev Anal Chem. https://doi.org/10.1080/10408347.2021.1889962
Sun Y, Zhao Z, Zhou R, Li P, Zhang W, Suematsu K, Hu J (2021) Synthesis of In_2O_3 nanocubes, nanocube clusters, and nanocubes-embedded Au nanoparticles for conductometric CO sensors. Sens Actuators B Chem 345:130433
Vizzini P, Manzano M, Farre C, Meylheuc T, Chaix C, Ramarao N, Vidic J (2021) Highly sensitive detection of *Campylobacter* spp. In chicken meat using a silica nanoparticle enhanced dot blot DNA biosensor. Biosens Bioelectron 171:112689
Wan C, Jiao Y, Qiang T, Li J (2017) Cellulose-derived carbon aerogels supported goethite (α-FeOOH) nanoneedles and nanoflowers for electromagnetic interference shielding. Carbohyd Polym 156:427–434
Xu W, Xue W, Huang H, Wang J, Zhong C, Mei D (2021) Morphology controlled synthesis of α-Fe_2O_3-x with benzimidazole-modified Fe-MOFs for enhanced photo-Fenton-like catalysis. Appl Catal B 291:120129
Yin IX, Zhang J, Zhao IS, Mei ML, Li Q, Chu CH (2020) The antibacterial mechanism of silver nanoparticles and its application in dentistry. Int J Nanomed 15:2555
Zhang M, Song Z, Liu H, Wang A, Shao S (2021) MoO_2 coated few layers of MoS_2 and FeS_2 nanoflower decorated S-doped graphene interoverlapped network for high-energy asymmetric supercapacitor. J Colloid Interface Sci 584:418–428
Zhou H, Mayorga-Martinez CC, Pané S, Zhang L, Pumera M (2021) Magnetically driven micro and nanorobots. Chem Rev 121(8):4999–5041

Publisher's Note Springer Nature remains neutral with regard to jurisdictional claims in published maps and institutional affiliations.

Springer Nature or its licensor (e.g. a society or other partner) holds exclusive rights to this article under a publishing agreement with the author(s) or other rightsholder(s); author self-archiving of the accepted manuscript version of this article is solely governed by the terms of such publishing agreement and applicable law.